Design and Installation of a New Electron Cyclotron Emission Diagnostic Antenna in LHD*)

Hayato TSUCHIYA, Yoshio NAGAYAMA, Kazuo KAWAHATA, Shigeru INAGAKI[1)], Shin KUBO and LHD Experiment Group

National Institute for Fusion Science, Toki 509-5292, Japan
[1)]*Research Institute for Applied Mechanics, Kyushu University, Kasuga 816-8580, Japan*

(Received 22 December 2010 / Accepted 19 May 2011)

A new electron cyclotron emission (ECE) antenna was designed and installed outside of torus, when the heating and diagnostics systems were reconfigured in LHD. Its design is based on Gaussian beam optics and consists of two plane and two concave mirrors. The mirror surfaces are defined using the concept of constant phase to improve matching to the corrugated waveguide. The new ECE antenna was used in a 2010 experiment to measure the electron temperature profile and its fluctuations.

Keywords: ECE, electron temperature, constant phase mirror, Gaussian beam, LHD

DOI: 10.1585/pfr.6.2402114

1. Introduction

Electron cyclotron emission (ECE) diagnostics [1] are important basic measurements in plasma diagnostics. Because ECE diagnostics have high spatial and temporal resolution, the electron profile and its fluctuations measured by ECE have been used in studies of magnetohydrodynamics (MHD), and heat transport in the Large Helical Device (LHD). For the 14th campaign (2010), a new ECE antenna was designed and installed in conjunction with a reconfiguration of the LHD's heating and measurement systems. This paper reports the design of the antenna system and the ECE measurement area in the LHD.

2. Antenna Systems

The new sight line is on the midplane outside of the torus. The helical magnetic configuration has a magnetic field peak around the center of the plasma, unlike that of tokamaks. A magnetic field peak appears around $R = 3.5$ m along the ECE sight line in the LHD. Therefore, only the outer half of the plasma can be measured using the outer ECE antenna.

Figure 1 shows a schematic of the layout of the ECE antenna system. The antenna consists of four ellipsoidal mirrors, M1, M2, M3, and M4. A fine-tuning mechanism is provided. To improve the measured microwave intensity, it is desirable to enlarge M4, which faces the plasma. The sizes of the mirrors are as follows: M1: 8 cm × 11 cm (in air), M2: 8 cm × 11 cm (in air), M3: 21 cm × 29 cm (in vacuum), and M4: 27 cm × 37 cm (in vacuum). M1 and M3 are plane mirrors, whereas M2 and M4 are concave mirrors. The use of two concave mirrors increases the degrees of freedom of the beam radius design. M4 is

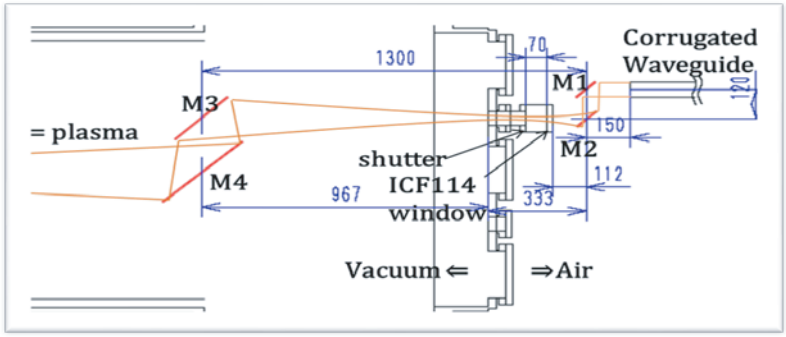

Fig. 1 Schematic layout plan of the ECE antenna system in the outer port of the torus in the LHD. The antenna consists of four mirrors, namely, M1, M2, M3, and M4 in the increasing order of distance from the waveguide in air. The layout is determined by the spot size at the plasma and the beam is passed through the tube between M2 and M3, matching it to the corrugated waveguide.

author's e-mail: tsuchiya.hayato@lhd.nifs.ac.jp

*) This article is based on the presentation at the 20th International Toki Conference (ITC20).

subjected to the ECE from the plasma, and the beam is tapered to pass through a tube with diameter 60 mm. After passing the shutter and the vacuum window, M2 matches the beam to the waveguide.

3. Constant Phase Mirror

The ECE, with a frequency of more than 50 GHz, is transported according the quasi-optical phenomenon. The corrugated waveguide, with inside diameter of 63.5 mm, matches well with the Gaussian beam. To improve the coupling, the surface of the concave mirrors is designed using the constant phase concept [2]. We consider the Gaussian beams incident on and reflected from a mirror when the waist size $w_{0,\mathrm{in}}$, $w_{0,\mathrm{out}}$ and waist position $r_{\mathrm{w,in}}$, $r_{\mathrm{w,out}}$ are known. The phase Ψ at position $\boldsymbol{r}$ is expressed as follows [3]:

$$\psi_{\mathrm{in}}(\boldsymbol{r}) = k\boldsymbol{r}\cdot\boldsymbol{e}_{\mathrm{in}} - \eta\left((\boldsymbol{r}-\boldsymbol{r}_{\mathrm{w,in}})\cdot\boldsymbol{e}_{\mathrm{in}}, w_{0,\mathrm{in}}\right) + \frac{k\left(\left|\boldsymbol{r}-\boldsymbol{r}_{\mathrm{w,in}}\right|^2 - \left|(\boldsymbol{r}-\boldsymbol{r}_{\mathrm{w,in}})\cdot\boldsymbol{e}_{\mathrm{in}}\right|^2\right)}{2R\left((\boldsymbol{r}-\boldsymbol{r}_{\mathrm{w,in}})\boldsymbol{e}_{\mathrm{in}}, w_{0,\mathrm{in}}\right)}, \quad (1)$$

and

$$\psi_{\mathrm{out}}(\boldsymbol{r}) = k\boldsymbol{r}\cdot\boldsymbol{e}_{\mathrm{out}} - \eta\left((\boldsymbol{r}-\boldsymbol{r}_{\mathrm{w,out}})\cdot\boldsymbol{e}_{\mathrm{out}}, w_{0,\mathrm{out}}\right) + \frac{k\left(\left|\boldsymbol{r}-\boldsymbol{r}_{\mathrm{w,out}}\right|^2 - \left|(\boldsymbol{r}-\boldsymbol{r}_{\mathrm{w,out}})\cdot\boldsymbol{e}_{\mathrm{out}}\right|^2\right)}{2R\left((\boldsymbol{r}-\boldsymbol{r}_{\mathrm{w,out}})\boldsymbol{e}_{\mathrm{out}}, w_{0,\mathrm{out}}\right)}. \quad (2)$$

Here, $k = 2\pi/\lambda$ is the wavenumber in free space; $\boldsymbol{e}_{\mathrm{in}}$ and $\boldsymbol{e}_{\mathrm{out}}$ are the propagating directional vectors. η is the phase shift term, and R is the radius of curvature. These functions of the distance from the waist position to the mirror z and the waist size are given by

$$\phi(z, w_0) = \tan^{-1}\left(\frac{\lambda z}{\pi w_0^2}\right), \quad (3)$$

and

$$R(z, w_0) = z + \frac{\left(\pi w_0^2/\lambda\right)^2}{z}. \quad (4)$$

Because the beam radius is a function of distance from the waist position, the values of $w_{0,\mathrm{in}}$, $w_{0,\mathrm{out}}$, $r_{\mathrm{w,in}}$, and $r_{\mathrm{w,out}}$ are required to match the waist size at the mirror position. If the matching is satisfied, the mirror surface can be numerically designed using the concept of constant phase given by the following relation [2]:

$$\psi_{\mathrm{in}}(\boldsymbol{r}) + \psi_{\mathrm{out}}(\boldsymbol{r}) = \text{constant}. \quad (5)$$

The surface of a mirror is numerically defined and it satisfies the reflection condition.

The use of more than one constant phase mirror allows us to freely design the waist size. Next, as an example, the matching of two constant-phase mirrors is considered when the distance L between the mirrors and the waist sizes w_1, w_2 at each mirror are given. The matching conditions satisfy the following relations when a beam waist exists between the two mirrors.

Here, w_0 is the waist size and z_1, z_2 are the distances from each mirror to the waist position. Noting

$$z_1 = \frac{\pi w_0}{\lambda}\left[w_1^2 - w_0^2\right]^{0.5}, \quad (6)$$

$$z_2 = \frac{\pi w_0}{\lambda}\left[w_2^2 - w_0^2\right]^{0.5}, \quad (7)$$

$$L = z_1 + z_2, \quad (8)$$

that the waist size has a positive value, we can solve for w_0:

$$w_0^2 = \frac{-as + 2a\sqrt{c-a^2}}{4c - s^2 - 4a}. \quad (9)$$

To simplify the equation, the following proxy constants are used:

$$c = w_1^2 w_2^2, \quad s = w_1^2 + w_2^2, \quad a = L^2\lambda^2/\pi^2. \quad (10)$$

Using the obtained waist size, we can easily derive z_1 and z_2.

4. Design of the Beam Radius and the Concave Mirror Surface

The beam radius is determined by the abovementioned equations. The conditions in the LHD are as follows: the measurement point is assumed to be the plasma center, the mirror size is larger than that at 1.1σ, and there are no obstacles within 1.5σ of free space. Here, σ is the width at which the beam intensity is $1/e^2$ of that at the beam center. The reference frequency used for optimization is 60 GHz, at which the beam spreads more rapidly than a higher-frequency wave. Figure 2 shows the beam radius evolution along the beam path z, where $z = 0$ corresponds to the position at the edge of the corrugated waveguide. The beam

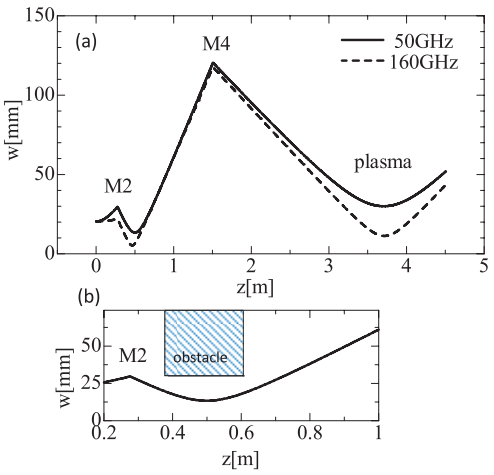

Fig. 2 (a) Beam size evolution at 50 GHz and 160 GHz. (b) Enlarged view around the waist position in a narrow tube. Stainless steel pipe 30 mm in radius is depicted as an obstacle.

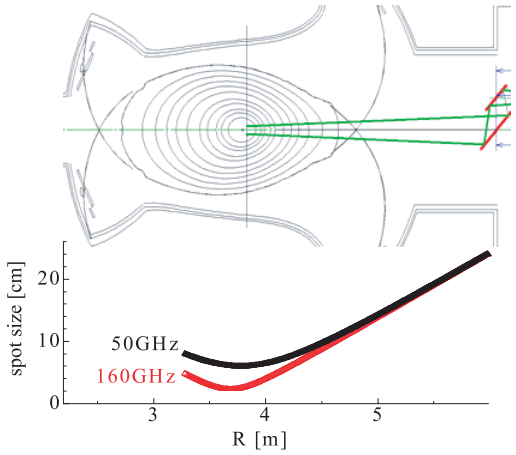

Fig. 3 Spot size at 50 GHz and 160 GHz in the plasma area. Waist position is set around the magnetic axis.

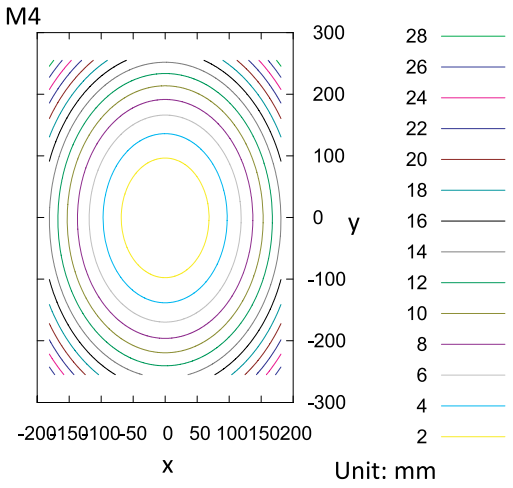

Fig. 4 Constant-phase mirror surface of M4. The value of contour lines is the height from the bottom at the center.

waist size is set to be 64.3% of the internal radius of the corrugated waveguide. The beam is tapered by matching M2 and M4 in order to pass it though the tube located at z = 388-609 mm. The beam waist is set at the center of the tube, i.e., z = 499 mm, so that the tube does not cut the beam at 1.5σ. Figure 3 graphs shows the spot size in the plasma area and a cross-sectional view of the vacuum vessel with a Poincaré plot of magnetic field lines. The spot size is defined as twice the beam radius and corresponds to the spatial resolution in the poloidal and toroidal directions. The waist position is set around the magnetic axis. The graph presents the spot sizes at 50 GHz and 160 GHz, which are the lower and upper frequency limits, respectively, under the LHD's experimental conditions. In the measurement area R = 4.0-4.8 m, the spot size is approximately 8 cm.

Figure 4 shows the calculated mirror surface of M4. The top and bottom surfaces of the mirror are asymmetrical. The mirrors are made of aluminum 5052 and their

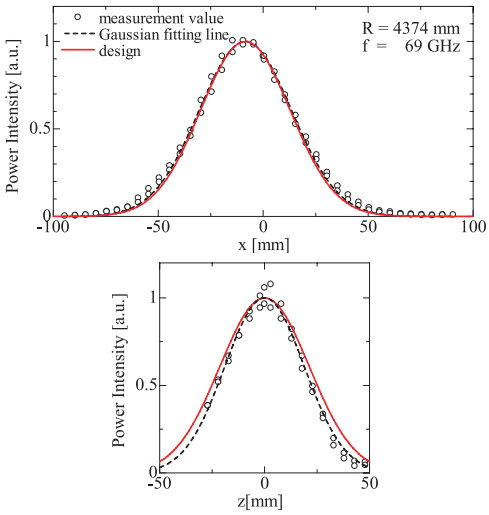

Fig. 5 Comparison between the measured power profile and the Gaussian beam profile. Intensity is normalized by the maximum of a fixed line of a measured value.

surfaces are formed by numerical control machining. After machining, the surface is polished and coated with Ni.

The beam profile was investigated in the LHD as shown in Fig. 5. A test wave with a frequency of 69 GHz was injected from the position of the corrugated waveguide. The power intensity was measured by a power monitor with a horn antenna at R = 4374 mm. The designed value of the spot size at that condition is 60.5 mm. Furthermore, the measured spot size was 62.2 mm in x-direction and 53.7 mm in z-direction. x-direction corresponds to the toroidal direction and z-direction is the vertical direction in the LHD. A side lobe is also found outside of 2σ However, its power is so low that its effect on the ECE measurement is negligible. The transmission ratio of the antenna system, including the vacuum window and the four mirrors, was found to be −7.6 +/− 0.1 dB and that of the waveguide system, which includes an approximately 100 m corrugated waveguide and more than 20 miter bends, was found to be −2.5 +/− 0.1 dB.

5. ECE Measurement Area in the LHD

A heliotron-type magnetic configuration has a saddle-shaped non-uniformity in the magnetic field strength across the poloidal cross section, and the magnetic field has a local maximum around R = 3.5 m on the sight line of the ECE measurement. Thus, the ECE from the outer half of the plasma column (R > 3.5 m) can reach the outer ECE antenna when the plasma is optically thick. Figure 6 shows the basic results of the ECE measurement. Figure 6 (a) shows the optical depth profile at B_{ax} = 2.75 T, $n_e(0)$ = 2.0 × 10^{18} m^3, and $T_e(0)$ = 2.0 keV. The derivation of the optical depth (τ) of the second harmonic X-mode uses the following equation [4].

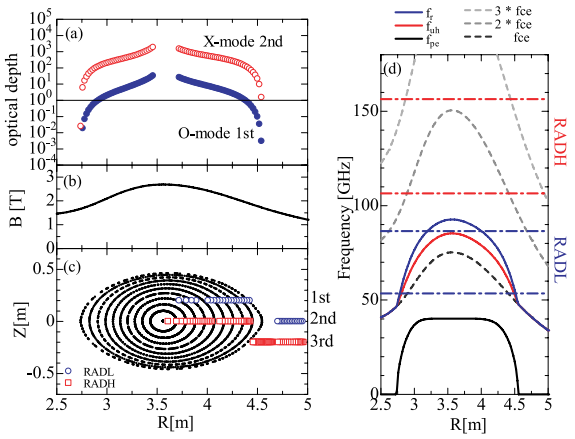

Fig. 6 (a) Optical depth profile. (b) Magnetic field profile along the ECE sight line. (c) Locations of the measurement points on the heterodyne radiometer channel. Sight line is on the midplane. Fundamental and third harmonic resonance points are drawn on the upper and lower lines to facilitate visualization. (d) Characteristic frequency profiles f_r: right hand cutoff frequency; f_{uh}: upper hybrid resonance frequency; f_{pe}: plasma frequency.

$$\tau_n^{\mathrm{x}} = \frac{\pi^2 n^{2(n-1)}}{2^{n-1}\,(n-1)!}\left(\frac{\omega_{\mathrm{pe}}}{\omega_{\mathrm{ce}}}\right)^2\left(\frac{v_{\mathrm{te}}}{c}\right)^{2(n-1)} \times\left(1 - C_n\left(\frac{\omega_{\mathrm{pe}}}{\omega_{\mathrm{ce}}}\right)^2\right)\frac{L_{\mathrm{B}}}{\lambda_0} \quad (n=2)\,. \tag{11}$$

Here,

$$C_{\mathrm{n}} = \left(n - \frac{3}{2} - \frac{2}{n}\right)\Big/\left(n^2 - 1\right) \quad (n=2)\,, \tag{12}$$

and $L_{\mathrm{B}} = B_0/|\mathrm{d}B_0/\mathrm{d}r|$; $\lambda_0 = 2\pi c/\omega_{\mathrm{ce}}$. The optical depth of the second harmonic X-mode is more than 1 in the $\rho > 0$ area. Because the magnetic gradient is quite small around $\rho \sim 0$ [Fig. 6 (b)], we must take care when applying the equation. In addition, a relativistic frequency downshift appears at $\rho < 0.1$ [5] when a high electron temperature is measured. When the frequency downshift occurs, the measurement point moves to the outer region.

The ECE is divided between a heterodyne radiometer and a Michelson interferometer by a beam splitter that uses a 10-μm wire grid. Two multi-channel filter banks for low frequency (53-84 GHz) and high frequency (106-156 GHz) are used in the radiometer, which has a frequency resolution of 1 GHz and a temporal resolution of 100 kHz. The radiometer, when used in conjunction with a low-frequency filter bank, [RadL in Fig. 6 (d)] is suitable for measuring temperature fluctuations when the magnetic field strength is 1.3-1.7 T. The radiometer is used with a high-frequency filter bank (RadH in the figure) when the magnetic field strength is greater than 2.2 T.

Figure 6 (c) shows an example of the measurement point configuration at $B_{\mathrm{ax}} = 2.75$ T. RadH covers most of the outer region and RadL can receive the fundamental harmonic of the O mode. The fundamental and second harmonics of the X mode do not overlap, as shown in Fig. 6 (d). Therefore, the second harmonic of the X mode is proportional to the electron temperature.

6. Summary

In summary, a new ECE antenna was designed and installed at the outside of the LHD torus. The beam evolution and mirror design were determined by quasi-optical equations. The spot size at the LHD plasma is approximately 8 cm, which corresponds to the spatial resolution. The measured spot size is confirmed to be consistent with the designed value. The new ECE antenna in conjunction with a heterodyne radiometer and a Michelson interferometer was used in a 2010 experiment to measure the electron temperature fluctuations.

Acknowledgment

This work was supported by the NIFS budget (NIFS10ULPP008, NIFS10ULPP020).

[1] Y. Nagayama, K. Kawahata, A. England, Y. Ito *et al.*, Rev. Sci. Instrum. **70**, 1021 (1999).
[2] S. Kubo *et al.*, Fusion Eng. Des. **26**, 319 (1995).
[3] P.F. Goldsmith, *Quasioptical Systems* (Wiley, New York, 1997).
[4] M. Bornatici *et al.*, Plasma. Phys. **23**, 1127 (1981).
[5] M. Sato *et al.*, Rev. Sci. Instrum. **75**, 3819 (2004).